Electrochimica Acta 129 (2014) 93–99

Contents lists available at ScienceDirect

Electrochimica Acta

journal homepage: www.elsevier.com/locate/electacta

Preparation and Electrochemical properties of Fe-Sn (C) Nanocomposites as Anode for Lithium-ion Batteries

Chun-jing Liu [a], Fang-hong Xue [a,*], Hao Huang [a], Xiu-hong Yu [a], Chang-jiang Xie [a], Meng-shi Shi [a], Guo-zhong Cao [a,b], Young-guan Jung [c], Xing-long Dong [a,*]

[a] School of Materials Science and Engineering, Key Laboratory of Materials Modification by Laser, Ion, and Electron Beams, Dalian University of Technology, Dalian 116023, China
[b] Department of Materials Science and Engineering, University of Washington, Seattle, WA 98195, USA
[c] Department of Mechanical Engineering, Kumoh National Institute of Technology, Daehakro 53, Gumi, Gyeong-Buk, 730-701, Republic of Korea

ARTICLE INFO

Article history:
Received 11 December 2013
Received in revised form 6 February 2014
Accepted 7 February 2014
Available online 4 March 2014

Keywords:
Lithium-ion Battery
Fe-Sn/C Nanocomposites
Arc-discharge method
Cycleability
Anode

ABSTRACT

In this work, Fe-Sn nanoparticles and its carbide counterpart, *i.e.* Fe-Sn/C nanoparticles were fabricated by DC arc-discharge method. The crystal structures, morphologies and cyclic performances of both samples were characterized by XRD, HRTEM and galvanostatic discharge/charge measurements. It is indicated that the main phases in two kinds of nanoparticles are $FeSn_2$ and Sn. The sizes of Fe-Sn nanoparticles are in the range of 30~100 nm, while Fe-Sn/C nanoparticles are about 10~50 nm. Fe-Sn nanoparticles electrode exhibits the real discharge/charge specific capacities of 192/159 mAh g^{-1}, those are gradually faded to near 11 mAh g^{-1} after 50 cycles. Nevertheless, Fe-Sn/C nanoparticles electrode has the real discharge/charge specific capacities of 557/517 mAh g^{-1}, can maintain to 373 mAh g^{-1} after 50 cycles. The carbon additive in Fe-Sn/C nanoparticles was characterized to be a graphite-like shell, its excellent effects on suppression of the volume change and electrochemical performances were discussed.

1. Introduction

Rechargeable lithium-ion batteries (LIB) now dominate the most of today's portable electronic market for their high energy density and high voltage [1,2]. Although carbonaceous materials have been the most widely used as the anode materials in commercial LIB, they are not sufficient to meet the needs of high-energy applications because of its relatively low capacity of 372 mAh g^{-1}. The searching for large-capacity and cyclic stable new LIB anode materials has become one of the main directions in the current study.

Tin has been suggested as an alternative anode material for LIB, as it forms a high atomic ratio compound ($Li_{4.4}Sn$) with Li, and thus leads to much high theoretical capacity (992 mAh g^{-1} [3]). However, the major problem is the severe volume change (>300% [3]) during discharge/charge cycles; it results in pulverization of the particles. One strategy has been proposed to buffer the volume change and improve the cycling performance of the Li alloy systems. It could use tin-based intermetallics M_xSn_y, where M is the electrochemically inactive transition metal, such as Sn-Ni alloys [4,5], Sn-Co alloys [6], Sn-Cu alloys [7], Sn-Sb alloys [8], and so on. During the discharge/charge processes, Sn atoms in these alloys will be dispersed into the inactive matrix and can inhibit the volume change. Carbon materials were also applied to the composites stabilizing the structures, the effects of carbon on the microstructure and electrochemical properties of nanocomposite LIB anode materials is an important topic that has attracted considerable attention in recent years. For example, the Fe-Sn/C system was first investigated in the 1990s. The Fe-Sn/C system particles synthesized by mechanical alloying methods or by direct melting of elemental powders had exhibited 600, 50, 20, and 60 mAh g^{-1}, respectively, for $FeSn_2$, FeSn, Fe_3Sn_2, and Fe_5Sn_3 [9–11]. $FeSn_2$/C nanocomposites synthesized by mechanical milling method had exhibited about specific capacity of 400 mAh g^{-1} after 35 cycles and then declined abrupt to less than 50 mAh g^{-1} after 50 cycles [12]. The Sn-Fe/C nanocomposites synthesized by a mechano-chemical method had exhibited about specific capacity of 380 mAh g^{-1} after 100 cycles [13].

In this study, a way to solve the volume change of alloys was investigated, that was to introduce carbon component into the Fe-Sn intermetallic compounds. Based on this proposal, DC arc-discharge method was adopted to fabricate Fe-Sn and Fe-Sn/C

* Corresponding author. Tel.: +86 411 8470 6130.
E-mail addresses: fhxue@dlut.edu.cn (F.-h. Xue), dongxl@dlut.edu.cn (X.-l. Dong).

http://dx.doi.org/10.1016/j.electacta.2014.02.031
0013-4686/

nanoparticles. Effects of the carbon on formation of core/shell nanocapsules and inhibition of the volume change were emphasized.

2. Experimental

2.1. Synthesis of Fe-Sn and Fe-Sn/C nanoparticles

Fe-Sn and Fe-Sn/C nanoparticles were synthesized by DC arc-discharge plasma as reported in our previous work [14]. The raw materials were micro-sized powder of pure metal Fe and Sn, these were mixed uniformly according to a mass ratio of 3:2 for Fe and Sn, and then compressed into a cylindrical bulk which would act as the anode of arc-discharge devices, meanwhile, tungsten rod served as the cathode. The arc-discharge was operated in a mixture atmosphere of argon and hydrogen (or methane) maintaining the current at 90 A. After a passivation process for 12 h, the nanopowders were collected from the chamber. For two kinds of nanoparticles, the only different in preparation conditions is the atmosphere, *e.g.* the mixture of argon and hydrogen was used for Fe-Sn nanoparticles (sample a) and the mixture of argon and methane for Fe-Sn/C nanoparticles (sample b).

2.2. Characterizations and electrochemical measurements

The crystal structure was characterized by X-ray diffraction (XRD-6000) using Cu Ka radiation (λ=1.5416 Å) at the scale of 20°~80°. The morphology and microstructure of the nanoparticles were analyzed using transmission electron microscopy (TEM, Tecnai220 S-TWIM). The component of element was characterized by X-Ray Fluorescence Spectrometer (XRF-1800). Cycling properties were performed by Land CT2001A. Cyclic voltammetric (CV) measurements and electrochemical impedance spectroscopic (EIS) of the electrodes were performed on a CHI660D electrochemical workstation.

The test electrode consisted of active powder material (Fe-Sn or Fe-Sn/C nanoparticles) (80 wt.%), conducting agent (carbon black) (10 wt.%) and polyvinylidene fluoride (PVDF, 10 wt.%) dissolved in N-methyl pyrrolidinone (NMP) as a binder. All of these components were mixed together thoroughly to form slurry, and then coated onto copper foil substrates. These sheets were dried under vacuum at 120 °C for 24 h and then used as the test electrodes. The half-cells were assembled in an argon-filled glove box. The metallic lithium sheet was used as the counter electrode, 1 M $LiPF_6$ in ethylene carbonate (EC)/diethyl carbonate (DEC) (1:1, v/v) as the electrolyte, and a polypropylene (PP) film as the separator. The charge/discharge behaviors were performed galvanostatically with a voltage window of 0.01 - 2.00 V (*vs.* Li/Li^+) at a current of 100 mA g^{-1}. Cyclic voltammetric (CV) measurements of the electrodes were performed with a scan rate of 0.1 mV s^{-1} between 0.01 - 2.00 V. EIS was carried out at a 5 mV amplitude signal in the frequency range of 0.01 Hz~100 KHz.

3. Results and Discussion

3.1. Crystal structures and morphologies of Fe-Sn and Fe-Sn/C nanoparticles

Fig. 1 shows the XRD patterns of Fe-Sn nanoparticles (sample a) and Fe-Sn/C nanoparticles (sample b). Both of them are of multi-phase containing $FeSn_2$ and Sn as the main phases. In Fe-Sn nanoparticles (sample a), besides the pure Sn phase, one can find two kinds of intermetallic compounds and one oxide, *i.e.* $FeSn_2$, FeSn and $Fe_{2.8}Sn_{0.2}O_4$. In Fe-Sn/C nanoparticles (sample b), the excess Sn becomes the dominant phase and only one of

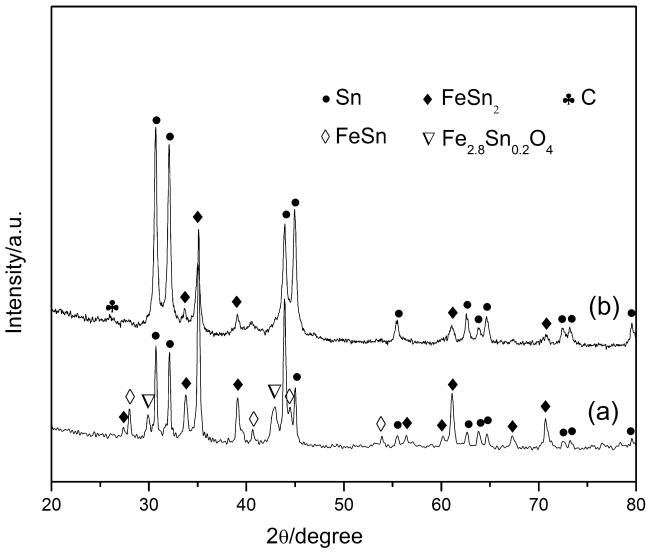

Fig. 1. XRD patterns of Fe-Sn nanoparticls (a) and Fe-Sn/C nanoparticles (b).

intermetallic compounds, $FeSn_2$, has been found. Comparison of the preparation conditions for two samples, it is interesting to find that carbon atoms significantly influence the phase formation and the species of intermetallic compounds through the nucleation and growth of nanoparticles. Furthermore, carbon atoms usually favor to form the shell of nanoparticles in a graphite-like structure, and can protect it from oxidization. The carbon shell in Fe-Sn/C nanoparticles will be further confirmed in the HRTEM analysis later in the paper.

Considering the excess of Sn and the absence of Fe phase in both samples a and b, it is thought that Fe source has been completely consumed in the formation of Fe-Sn intermetallic compounds. The process of arc discharge for fabricating nanoparticles is actually a typical physical vapor condensation and also a non-equilibrium process, in which the nucleation and growth of nanoparticles would occur through random collision. Generally, the formation of intermetallic compound follows the principle of minimum energy, depending on the effective formation heats of phases coexisted. It was known that the effective formation heats of $FeSn_2$ and FeSn phases are -0.087, -0.082 kJ/(mol·atom), respectively [15]. The primary phase is usually the most negative among all phases, hence $FeSn_2$ is possible to be dominant in two kinds of Fe-Sn and Fe-Sn/C nanoparticles. In other words, $FeSn_2$ can also be formed in spite of existence of the carbon atoms in the case for Fe-Sn/C nanoparticles, most probably due to (1) negligible difference in the formation energy and (2) insufficient diffusion of the constituent elements.

It has been confirmed that a small carbon peak can be detected by XRD measurement in Fe-Sn/C nanoparticles. Fe-Sn/C nanoparticles displayed the broad diffraction peaks in comparison with those of Fe-Sn nanoparticles, the mean particle size of Fe-Sn/C and Fe-Sn calculated from Scherrer equation to be around 38 nm and 52 nm, respectively, indicating carbon atoms may inhibit the growth of grains in nanoparticles. HRTEM analysis can supply further evidences for the reduced sizes and carbon-coated Fe-Sn/C nanostructures.

Fig. 2 shows the morphologies of Fe-Sn nanoparticles (Fig. 2, a1, a2) and Fe-Sn/C nanoparticles (Fig. 2, b1, b2). The average particle size of Fe-Sn nanoparticles is in the range of 30~100 nm. It is clear that the core is $FeSn_2$ multi-grained with lattice spacing of 0.267 nm for crystal plane (002) and 0.324 nm for (200) (PDF # 73-2030). The surface oxide on the Fe-Sn nanoparticles is amorphous with about 3 nm in shell thickness. EDS spot analysis profiles for Fe-Sn nanoparticles and Fe-Sn/C nanoparticles are exhibited in Fig. 2

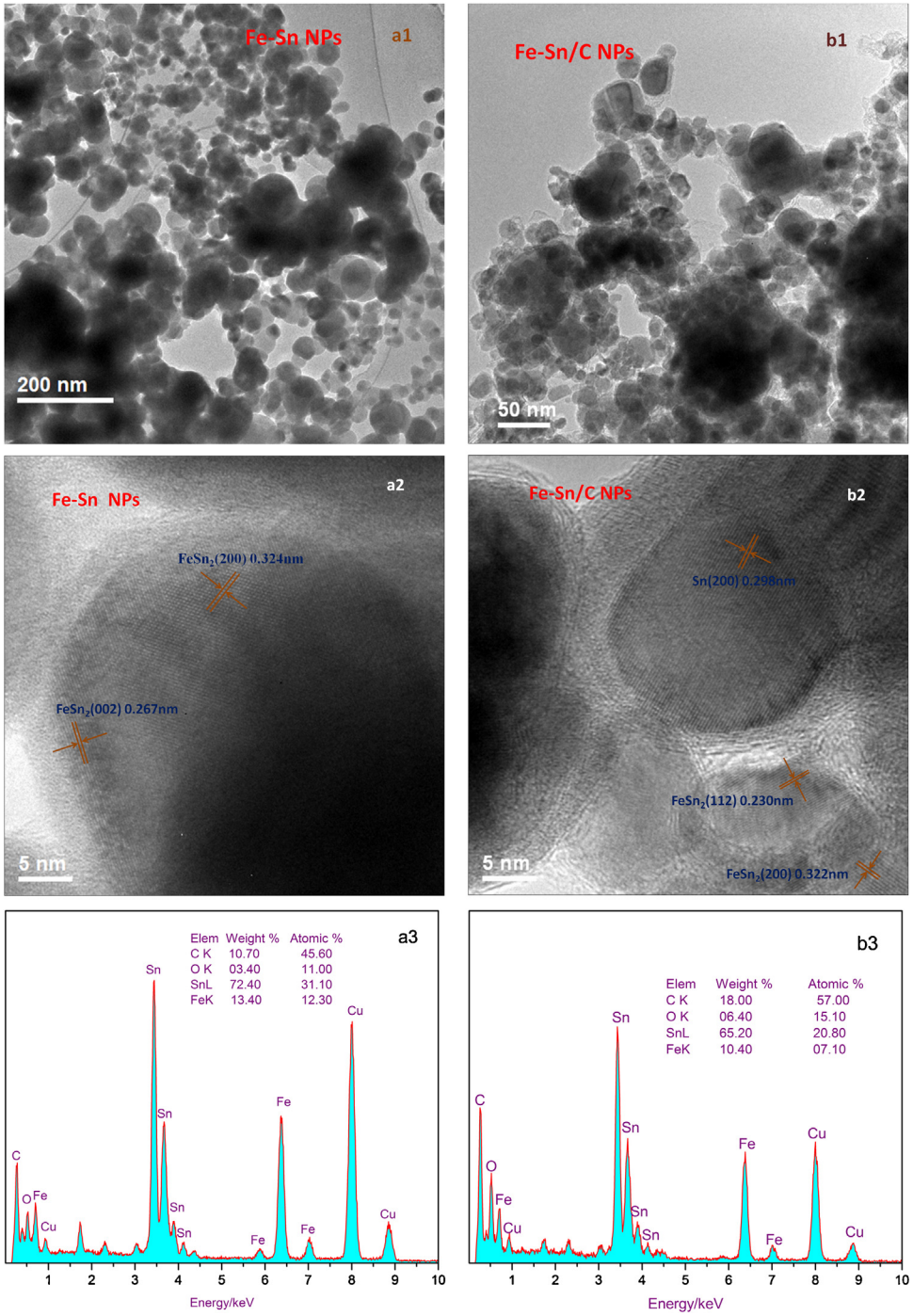

Fig. 2. (a1) TEM images of Fe-Sn nanoparticles. (a2) HRTEM images of Fe-Sn nanoparticles. (a3) EDS spot analysis profile for Fe-Sn nanoparticles. (b1) TEM images of Fe-Sn/C nanoparticles. (b2) HRTEM images of Fe-Sn/C nanoparticles. (b3) EDS spot analysis profile for Fe-Sn/C nanoparticles.

a3 and b3. The C peak for Fe-Sn nanoparticles and Cu peaks for both particles come from the copper foil to support the powders for TEM analysis. The O/Sn/Fe atomic ratio is 11: 31: 12 for the Fe-Sn particles, greatly exceeding the element ratio in $FeSn_2$. This indicates that element Fe fully alloyed with Sn and no metal peaks can be discerned in the XRD. The C/O/Sn/Fe atomic ratio is 57: 15: 21: 7 for the Fe-Sn/C particles, the O signal can be related to the oxygen adsorbed on the carbon during the sample preparation process [16]. The weight ratio of carbon is ~18% which is in a good agreement with the results of element analyze (~19%).

In contrast, the mean size of Fe-Sn/C nanoparticles is among 10~50 nm, which is apparently less than that of Fe-Sn nanoparticles, possibly attributable to the influence of carbon. It is observed that a graphite-like layer covers the surface of nanoparticles, indicating the existence of carbon phase and a carbon-coated nanostructure. In the inner of cores, the Sn grain with (200) plane and $FeSn_2$ with planes of (112) and (200) are observed. This configuration of the carbon-coated nanostructure agrees well with XRD results, and accord with the formation mechanism for the carbon-coated Fe and Co nanocapsules [17,18]. It is suggested that Fe or Co atoms can combine with carbon atoms to form a solid solution at high temperature and then dissolve out the supersaturated carbon to form a graphite-like shell on the surface of nanocapsules as cooling to room temperature. In the case of present Fe-Sn/C

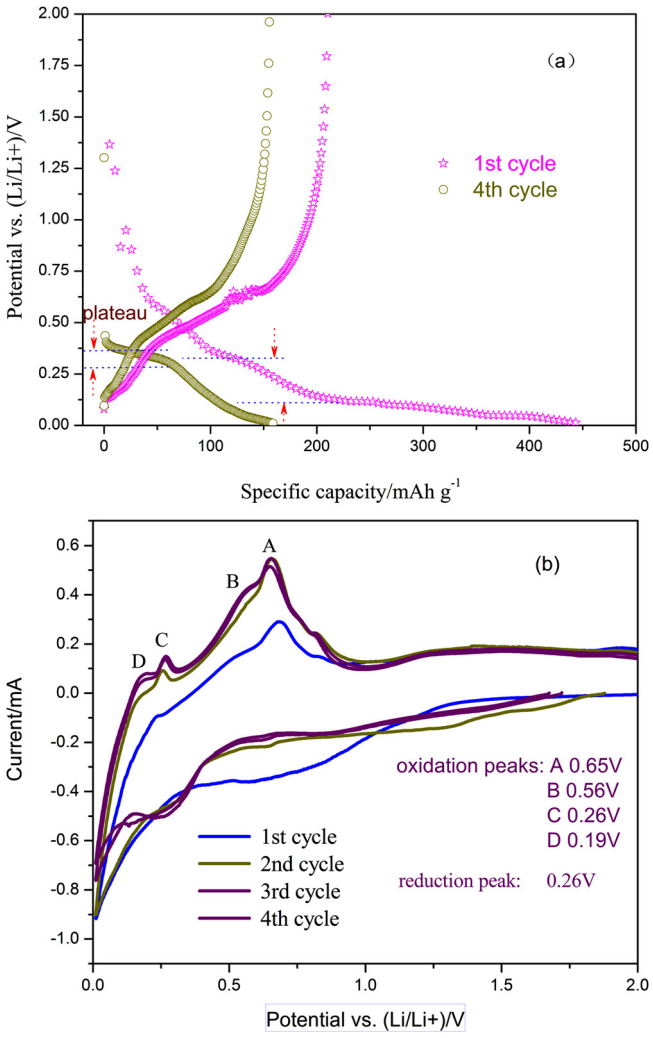

Fig. 3. (a) Discharge/charge curves of Fe-Sn nanoparticles electrode at a current density of 100 mA g-1 within a voltage window of 0.01-2.00 V. (b) CV curves of Fe-Sn nanoparticles electrode at scan rate of 0.1 mV s-1.

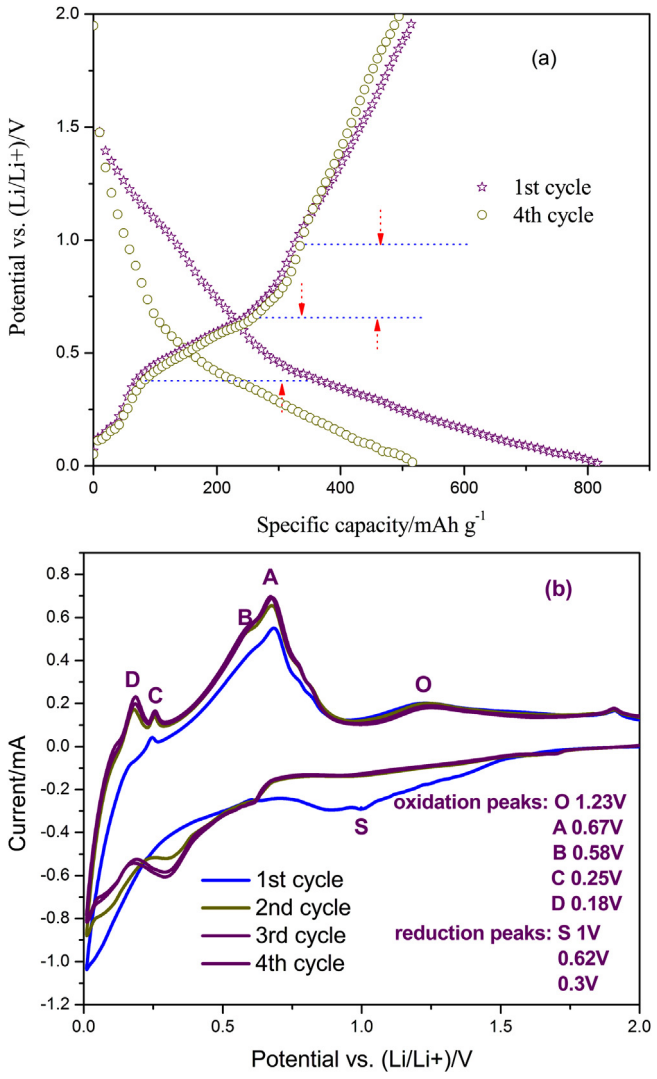

Fig. 4. (a) Discharge/charge curves of Fe-Sn/C nanoparticles electrode at a current density of 100 mA g-1 within a voltage window of 0.01-2.00 V. (b) CV curves of Fe-Sn/C nanoparticles electrode at scan rate of 0.1 mV s-1.

nanoparticles, methane was decomposed and formed the carbon shells of Fe-Sn/C nanocapsules.

3.2. *Electrochemical performance of Fe-Sn and Fe-Sn/C nanoparticles electrodes*

Using Fe-Sn and Fe-Sn/C nanoparticles as the active materials, the work electrodes were prepared and their electrochemical properties were measured in half-cells with lithium sheets as the counter electrodes. Fig. 3a shows the discharge/charge curves (for the first and fourth cycles) of Fe-Sn nanoparticles electrode at a current density of 100 mA g^{-1} within a voltage window of 0.01-2.00 V relative to Li/Li^+ metal. In the first charging, there are three plateaus at about 0.90, 0.60 and 0.30 V, however, the 0.90 V plateau disappears at following discharging which caused by the formation of solid electrolyte interphase (SEI) and results in the first-cycle irreversible capacity, as it is commonly observed and reported in literature [19]. Fig. 3b is the CV curves of Fe-Sn nanoparticles electrode at a scan rate of 0.1 mV s^{-1}, which are well matched with the reaction potentials (plateaus) observed in Fig. 3a. The reduction peak at about 1.00 V in the first discharging disappeared in the subsequent cycles, corresponding to the SEI formation. The other reduction peaks at about 0.60 V and 0.26 V relate to the alloying of Sn and Li [20], and the oxidation peaks (at 0.56 and 0.65 V) associate with the dealloying processes (Li_5Sn_2 and LiSn) [21,22].

Fig. 4a shows the discharge/charge curves (for the first and fourth cycles) of the Fe-Sn/C nanoparticles electrode at a current density of 100 mA g^{-1} within 0.01-2.00 V. Fig. 4b is CV curves of Fe-Sn/C nanoparticles electrode at scan rate of 0.1 mV s^{-1}. The two potentials (0.60, 0.30 V) are well consistent with that of Fe-Sn nanoparticles, but 0.10 V is a little higher than those in Fe-Sn nanoparticles electrode. Owing to the different surface states between Fe-Sn and Fe-Sn/C nanoparticles, one can easily understand the differences in the surface reaction processes. It is reasonable that 0.10 V corresponds to the formation of LiC_6 [23], and the oxidation peak at 1.23 V is a slight oxidation of Sn [24] or the adsorbed oxygen on the carbon, which was reflected by the EDS.

Fig. 5 presents the cycle behaviors of Fe-Sn (a) and Fe-Sn/C (b) nanoparticles electrodes at the current density of 100 mA g^{-1}. As shown in Fig. 5a, the first discharge capacity of Fe-Sn nanoparticles electrode is 449 mAh g^{-1}, its irreversible capacity is 212 mAh g^{-1}, and the Coulomb efficiency is 47.2%. After 50 cycles, the initial capacity decays to 11 mAh g^{-1} with great irreversible capacity losses. It is suggested that the large decrease of capacity for Fe-Sn nanoparticles electrode is caused by three reasons: first, the surface oxides on Fe-Sn nanoparticles may react with Li^+ to form lithium

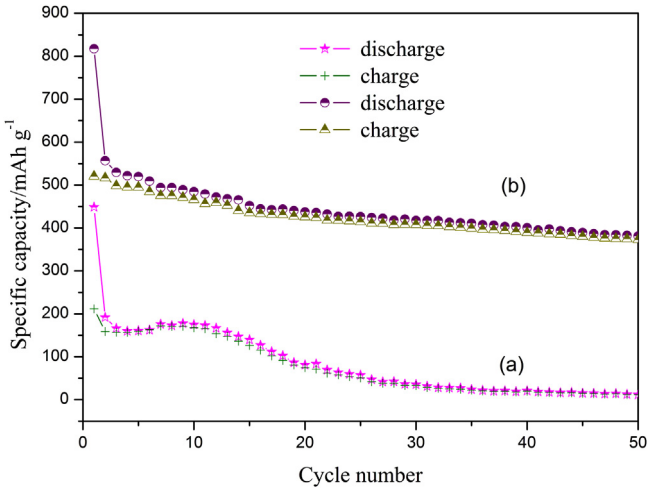

Fig. 5. Cycling behaviors of Fe-Sn (a) and Fe-Sn/C (b) nanoparticles electrodes at the current density of 100 mA g-1.

oxide (Li_2O), which is irreversible to release the ions; second, SEI passivation film is formed on the interfaces between active matters and electrolyte in the first discharge/charge process; third, as proved the amorphous oxide-coated Fe-Sn nanoparticles, it has a limited ability to restrain a great volume expansion/constriction during the intercalation/deintercalation of lithium ions [25], which may result in the cracking of active materials with new fresh surface, and subsequently more lithium ions are consumed to form new SEI, and finally, the large volume change may ultimately lead to mechanically disintegration of electrode material.

The first discharge capacity of Fe-Sn/C nanoparticles electrode is 818 mAh g^{-1} (Fig. 5b), its irreversible capacity is 520 mAh g^{-1}, and Coulomb efficiency is 63.6% (Fig. 5b). In comparison with the counterpart, the carbon-coated Fe-Sn/C nanoparticles electrode has high capacity retainability, maintaining to 373 mAh g^{-1} after 50 cycles. It is expected that the carbon-coated nanocapsules exhibit excellent cycling performance due to the protection and the stable interfaces by the graphite-like shells. Another favorable character of Fe-Sn/C nanoparticles is its smaller particles' size than Fe-Sn particles' which also can alleviate the volume expansion in the cycling. Yang et al. [26] had indicated the same phenomenon in Sn powders, as the particle size decreased from 3 μm to 300 nm, the number of stable cycles increased from 3 to 70.

3.3. *Impedance characteristics of Fe-Sn and Fe-Sn/C nanoparticles electrodes*

In order to gain further sight into the electrochemical performances of Fe-Sn and Fe-Sn/C nanoparticles electrodes, EIS measurements were carried out on initial electrodes at open-circuit voltage as well as the cycled electrodes. Fig. 6a is the Nyquist plots for Fe-Sn and Fe-Sn/C nanoparticles electrodes in the open circuit, and the inset is the equivalent analog circuits for both of the two electrodes in the open circuit. Fig. 6b is the selected Nyquist plots for Fe-Sn/C nanoparticles electrodes during cycles and the insets are the equivalent analog circuits and Nyquist plots for the electrode during the cycles. Fig. 6(c) is the Bode plots for Fe-Sn/C nanoparticles during the cycles and the fit curves. Where R_Ω refers to uncompensated resistance between working electrode and lithium reference electrode, CPE_s refers to constant phase element of the surface layer, R_s refers to the resistance of the SEI, and CPE_{dl} refers to the double layer, R_{ct} refers to charge transfer resistance, Z_W refers to Warburg impedance. The EIS data based on the equivalent circuits are given in Table 1.

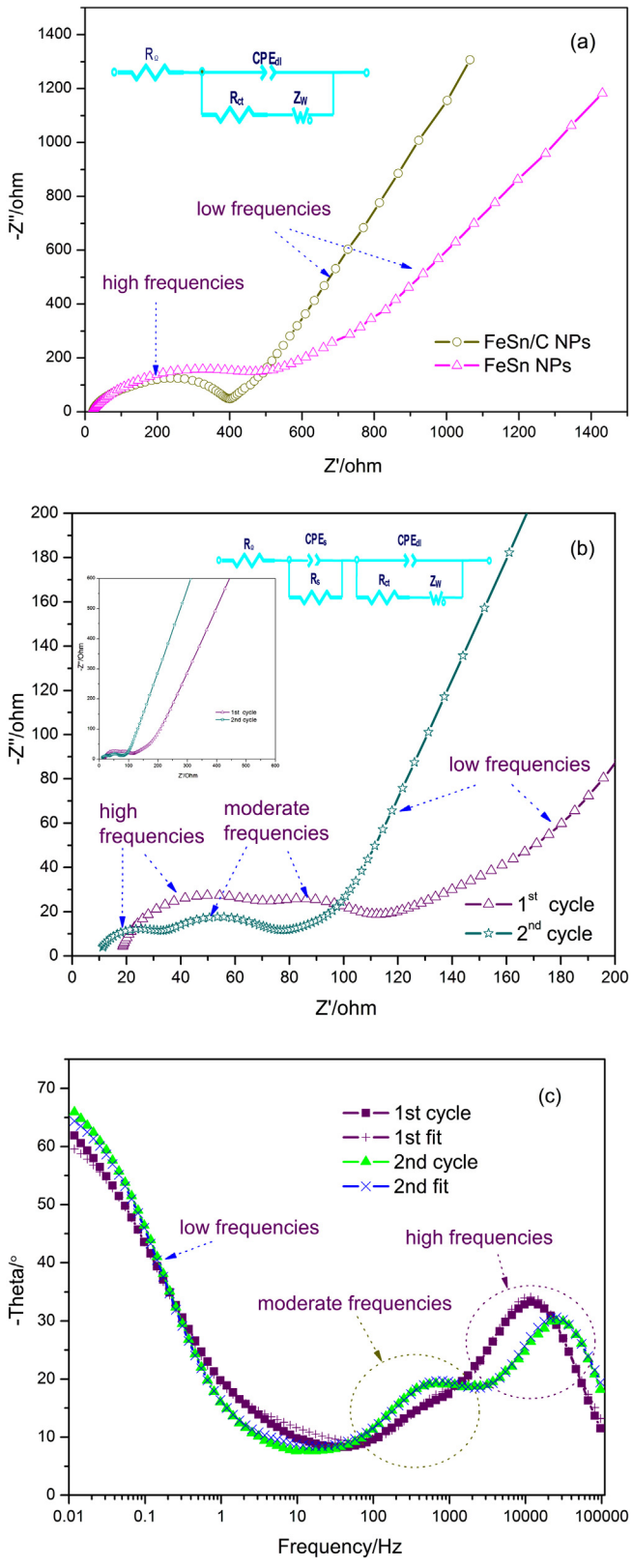

Fig. 6. (a) Nyquist plots of Fe-Sn and Fe-Sn/C nanoparticles electrodes in the open circuit, the inset is the equivalent analog circuits for both of the two electrodes. (b) The selected Nyquist plots for Fe-Sn/C nanoparticles electrodes during cycles and the insets are the equivalent analog circuits and Nyquist plots for the electrode during the cycles. (c) Bode plots for Fe-Sn/C nanoparticles during the cycles and the fit curves.

Table 1
Parameters of components in analog circuit.

	Fe-Sn/C anode electrode Open circuit	Fe-Sn/C anode electrode 1 cycle	Fe-Sn/C anode electrode 2 cycle	Fe-Sn anode electrode Open circuit
$R_\Omega(\Omega)$	18.14	17.51	9.97	16.46
$R_s(\Omega)$		60.64	23.91	
$R_{Ct}(\Omega)$	360.60	17.45	36.24	540.30
$D_0(cm^2\ s^{-1})$	9.31E-14	4.23E-13	1.17E-12	1.83E-14

In Nyquist plots and the Bode plots, the semicircle in high frequencies relates to the transport properties of the SEI film on the surface of electrode, a depressed semicircle in the moderate frequency region relates to the charge transfer process, and the inclined line in low frequency range is ascribe to the lithium-ion diffusion through inner active materials [27]. Compared to the diameters (the charge transfer resistance) of semicircles in high frequencies for the initial electrodes as shown in Fig. 6 (a) and the resistance data from Fig. 6 (a) also listed in Table 1, it is apparent that the charge transfer resistance of Fe-Sn/C nanoparticles electrode is much lower than that of Fe-Sn counterpart. The increased conductivity can be attributed to the conductive carbon shell on the surface of Fe-Sn/C nanoparticles [24]. The smaller size of Fe-Sn/C nanoparticles may also promote the free charge transfer at the large surface area between particles/electrolyte [28].

According to the formula [28]:

$$\sigma = RT\left[2^{1/2}An^2F^2(D_0C)^{1/2}\right]^{-1}$$

the diffusion coefficient of Li^+ D_0 can be concluded, where σ is Warburg coefficient, R is the gas constant, T is absolute temperature, A is the contact area between the electrolyte and the electrode, n is the number of electrons transferred per mole of a substance involved in the electrode reaction, F is the Faraday constant, C is concentration of lithium in the electrode.

For the initial electrodes, EIS measurements at open-circuit voltage means no SEI films were formed, but it will develop in the cycled electrodes. The two semicircles appear in Nyquist plots (Fig. 6 (b)) and Bode plots (Fig. 6 (c)) of the cycled electrodes for Fe-Sn/C sample. From the shapes of semicircles and the parameters given in Table 1, it shows the R_s decreased when the cycling is increase, it is probable linked to the thickness of the SEI layer which is assumed to be thinner [29]. The reduced R_{ct} allows better contact between the active materials and the electrolyte after 1 cycled, and achieves a high reaction area, so reduced the charge transfer resistance [30]. The reduced R_{ct} also improved abilities for Li^+ diffusion in the cycled electrodes. It was thought that the transpositional Fe and new Li-Sn phase can strengthen Li^+ transportation in the cycled electrodes [9].

The D_0 of the Fe-Sn electrode is much smaller than that of Fe-Sn/C electrode. It mainly attributed to the shorter diffusion path in Fe-Sn/C electrode [31], besides, the surface of the material particles also plays a key role on the diffusion coefficient.

4. Conclusions

Fe-Sn nanoparticles and Fe-Sn/C nanoparticles were fabricated successfully by a DC arc-discharge method. The main phases in both samples are $FeSn_2$ and Sn. The particle size of Fe-Sn nanoparticles is among 30∼100 nm, while Fe-Sn/C nanoparticles is in range of 10∼50 nm with a carbon-coated nanostructure. Fe-Sn nanoparticles electrode exhibits the real discharge/charge capacities of 192/159 mAh g^{-1} and decay to 11 mAh g^{-1} after 50 cycles. Fe-Sn/C nanoparticles electrode has the real discharge/charge capacities of 557/517 mAh g^{-1} and maintain to 373 mAh g^{-1} after 50 cycles. The excellent electrochemical performances of Fe-Sn/C nanoparticles are determined from the unique carbon-coated nanostructures and improved ability to restrain the volume change during intercalation/deintercalation of lithium ions.

Acknowledgments

This work was supported by the National Key Basic Research and Development Program (Grant No. 2011CB936002), the National Natural Science Foundation of China (No.51271044, 11004019 and 51171033) and the Fundamental Research Funds for the Central Universities (2012DUT12RC(3)101).

References

[1] P.L. Taberna, S. Mitra, P. Poizot, P. Simon, J.-M. Tarascon, High rate capabilities Fe_3O_4-based Cu nano-architectured electrodes for lithium-ion battery applications, Nat. Mater. 5 (2006) 567.
[2] K.S. Kang, Y.S. Meng, J. Bréger, C.P. Grey, G. Ceder, Electrodes with high power and high capacity for rechargeable lithium batteries, Science 311 (2006) 976.
[3] M.J. Noh, Y.J. Kwon, H.J. Lee, J. Cho, Y. Kim, M.G. Kim, Amorphous carbon-coated tin anode material for lithium secondary battery, Chem. Mater. 17 (2005) 1926.
[4] L. Huang, H.B. Wei, F.S. Ke, X.Y. Fan, J.T. Li, S.G. Sun, Electrodeposition and lithium storage performance of three-dimensional porous reticular Sn–Ni alloy electrodes, Electrochim. Acta 54 (2009) 2693.
[5] J. Hassoun, S. Panero, B. Scrosati, Electrodeposited Ni–Sn intermetallic electrodes for advanced lithium ion batteries, J. Power Sources 160 (2006) 1336.
[6] J.J. Zhang, Y.Y. Xia, Co-Sn alloys as negative electrode materials for rechargeable lithium batteries, J. Electrochem. Soc. 1538 (2006) A1466.
[7] W.H. Pu, X.M. He, J.G. Ren, C.R. Wan, C.Y. Jiang, Electro-deposition of Sn–Cu alloy anodes for lithium batteries, Electrochim. Acta 50 (2005) 4140.
[8] L.H. Shi, H. Li, Z.X. Wang, X.J. Huang, L.Q. Chen, Nano-SnSb alloy deposited on MCMB as an anode material for lithium ion batteries, J. Mater. Chem. 11 (2001) 1502.
[9] O. Mao, R.A. Dunlap, J.R. Dahn, Mechanically alloy Sn-Fe(-C) powders as anode materials for Li-Ion batteries I. The Sn_2Fe-C system, J. Electrochem. Soc. 146 (1999) 405.
[10] O. Mao, J.R. Dahn, Mechanically alloyed Sn-Fe(-C) powders as anode materials for Li-ion batteries II. The Sn-Fe system, J. Electrochem. Soc. 146 (1999) 414.
[11] O. Mao, J.R. Dahn, Mechanically alloyed Sn-Fe(-C) powders as anode materials for Li-ion batteries III. Sn_2Fe:$SnFe_3C$ Active/Inactive Composites, J. Electrochem. Soc. 146 (1999) 423.
[12] J.M. Lee, W.S. Chang, B.C. Yu, H. Kim, D. Im, Enhancement of cyclability using recombination reaction of Cu for Sn_2Fe nanocomposite anode for lithium-ion batteries, J. Electrochem. Commun. 12 (2010) 928.
[13] S.K. Yoon, J.M. Lee, H.S. Kim, D.M. Im, S.G. Doo, H.J. Sohn, An Sn–Fe/carbon nano composite as an alternative anode material for rechargeable lithium batteries, Electrochim. Acta 54 (2009) 2699.
[14] J.P. Lei, X.L. Dong, X.G. Zhu, M.K. Lei, H. Huang, X.F. Zhang, B. Lu, W.J. Park, H.S. Chung, Formation and characterization of intermetallic Fe-Sn nanoparticles synthesized by an arc discharge method, Intermetallics 15 (2007) 1589.
[15] J.P. Lei, X.L. Dong, F.G. Zhao, B. Lv, H. Huang, M.K. Lei, Prediction of the primary intermetallic compound nanoparticles formed in Fe(Ni)-Sn system, Acta Metall. Sinica 44 (2008) 922.
[16] B. Wang, X.L. Li, B. Luo, X.F. Zhang, Y.Y. Shang, A.Y. Cao, L.J. Zhi, Intertwined network of Si/C nanocables and carbon nanotubes as lithium-ion battery anodes, Appl. Mater. Interfaces 5 (2013) 6467.
[17] X.L. Dong, Z.D. Zhang, Q.F. Xiao, X.G. Zhao, Y.C. Chuang, S.R. Jin, W.M. Sun, Z.J. Li, Z.X. Zheng, H. Yang, Characterization of ultrafine γ-Fe(C),α-Fe(C) and Fe_3C particles synthesized by arc-discharge in methane, J. Mater. Sci. 35 (1998) 1915.
[18] X.L. Dong, Z.D. Zhang, Y.C. Chuang, S.R. Jin, Characteriztion of ultrafine Fe-Co particles and Fe-Co(C) nanocapsules, Phys. Rev. B 60 (1999) 3017.
[19] W.J. Zhang, A review of the electrochemical performance of alloy anodes for lithium- ion batteries, J. Power Sources 196 (2011) 13.
[20] S.K. Yoon, A. Manthiram, Nanostructured Sn-Ti-C composite anodes for lithium ion batteries, Electrochim. Acta 56 (2011) 3029.
[21] J.C. He, H.L. Zhao, J. Wang, J. Wang, J.B. Chen, Hydrothermal synthesis and electrochemical properties of nano-sized Co–Sn alloy anodes for lithium ion batteries, J. Alloys Compd. 508 (2010) 629.
[22] M. Winter, J.O. Besenhard, Electrochemical lithiation of tin and tin-based intermetallics and composites, Electrochim. Acta 45 (1999) 31.

[23] J.M. Lee, H.C. Jung, Y. Hwa, H.S. Kim, D.M. Im, S.G. Doo, H.J. Sohn, Improvement of electrochemical behavior of Sn_2Fe/C nanocomposite anode with Al_2O_3 addition for lithium-ion batteries, J. Power Sources 195 (2010) 5044.
[24] J.H. Kong, Z.L. Liu, Z.C. Yang, H.R. Tan, S.X. Xiong, S.Y. Wong, X. Li, X.H. Lu, Carbon/SnO_2/carbon core/shell/shell hybrid nano -fibers: tailored nanostructure for anode of lithium ion batteries with high reversibility and rate capacity, Nanoscale4 (2012) 525.
[25] X.H. Hou, S.J. Hu, W.S. Li, L.Z. Zhao, H.W. Yu, C.L. Tan, Investigation of lithiation/delithiation mechanism in Li-Sn alloys for anode materials, Chin. Phys. Soc. 57 (2008) 2734.
[26] J. Yang, M. Wachtler, M. Winter, J.O. Besenhard, Sub-Microcrystalline Sn and Sn-SnSb Powders as Lithium Storage Materials for Lithium-Ion Batteries, Electrochem. Solid-State Lett. 2 (1999) 161.
[27] S.D. Xu, Q.C. Zhuang, Y.L. Shi, Y.B. Zhu, X.Y. Qiu, Z. Sun, Electrochemical impedance spectra of intercalation compound electrodes: models and theoretical simulations, Acta Phys. -Chim. Sin. 27 (2011) 2353.
[28] H. Liu, G.X. Wang, J. Liu, S.Z. Qiao, H.J. Ahn, Highly ordered mesoporous NiO anode material for lithiumion batteries with an excellent electrochemical performance, J. Mater. Chem. 21 (2011) 3046.
[29] C. Marino, A. Darwiche, N. Dupré, H.A. Wilhelm, B. Lestriez, H. Martinez, R. Dedryvère, W. Zhang, F. Ghamouss, D. Lemordant, L. Monconduit, Study of the Electrode/Electrolyte Interface on Cycling of a Conversion Type Electrode Material in Li Batteries, J. Phys. Chem. C 117 (2013) 19302.
[30] Y. Xia, Z. Xiao, X. Dou, H. Huang, X.H. Lu, R.J. Yan, Y.P. Gan, W.J. Zhu, J.P. Tu, W.K. Zhang, X.Y. Tao, Green and Facile Fabrication of Hollow Porous MnO/C Microspheres from Microalgaes for Lithium-Ion Batteries, ACS Nano 7 (2013) 7083.
[31] Y. Cui, X.L. Zhao, R.S. Guo, Improved electrochemical performance of $La_{0.7}Sr_{0.3}MnO_3$ and carbon co-coated $LiFePO_4$ synthesized by freeze-drying process, Electrochim. Acta 55 (2010) 922.